Pure Appl. Chem., Vol. 83, No. 4, pp. 899–912, 2011.
doi:10.1351/PAC-CON-10-10-22

Engineering supramolecular photoactive nanomaterials by hydrogen-bonding interactions*

K. Yoosaf[1], Abdelhalim Belbakra[1], Anna Llanes-Pallas[2], Davide Bonifazi[2,3,‡], and Nicola Armaroli[1,‡]

[1]Molecular Photoscience Group, Istituto per la Sintesi Organica e la Fotoreattività, Consiglio Nazionale delle Ricerche (CNR-ISOF), Via Gobetti 101, 40129 Bologna, Italy; [2]INSTM UdR di Trieste and Dipartimento di Scienze Farmaceutiche, Università di Trieste, Piazzale Europa 1, 34127 Trieste, Italy; [3]Chemistry Department, University of Namur, Rue de Bruxelles 61, 5000 Namur, Belgium

Abstract: The photophysical properties of molecules containing anthracene, pyrene, or phenyleneethynylene chromophores bearing complementary triple H-bonding terminal units, namely, 2,6-di(acetylamino)pyridine (donor–acceptor–donor, DAD) and uracyl (acceptor–donor–acceptor, ADA) have been investigated as a function of solvent polarity. For asymmetric systems, presenting only one H-bonding unit, a solvatochromic effect is found, suggesting a charge-transfer character of the lowest electronic excited state. Systematic absorption and emission studies carried out as a function of temperature show that phenyleneethynylenes having linear geometry and H-bonding functionalities at both ends undergo reversible self-aggregation in cyclohexane (CHX), leading to the formation of spherical nanoparticles, as evidenced by wide-field fluorescence microscopy (WFM), atomic force microscopy (AFM), and transmission electron microscopy (TEM). A combination of an anthracene derivative bearing only one ADA terminal functionality and a linear phenyleneethynylene derivative possessing two DAD terminal groups in CHX (2:1 molecular ratio) leads to the formation of vesicular nanostructures. The interaction of linear phenyleneethynylenes possessing two terminal 2,6-di(acetylamino)pyridine functionalities with that bearing bis uracylic units gives origin to nanofibers, while the assembly of the former with bisuracylic units exhibiting bent geometry leads to the formation of helical nanofibers. The length of these fibers can be controlled by addition of the anthracene derivative having only one uracyl group which effectively blocks the extent of H-bonding, prompting the formation of shorter nanorods.

Keywords: hydrogen bonding; nanomaterials; photochemistry; self-assembly; supramolecular chemistry.

*Paper based on a presentation made at the XXIII[rd] IUPAC Symposium on Photochemistry, Ferrara, Italy, 11–16 July 2010. Other presentations are published in this issue, pp. 733–930.

‡Corresponding authors

INTRODUCTION

In the last few years, organic nanomaterials [1–5] have attracted much attention due to their potential applications in various fields such as light-emitting devices [6,7], solar cells [8–10], or polymer-based transistors [11–14]. Such interest is somewhat related to the fact that electronic and optical properties of organic nanomaterials are highly dependent on their size, shape, and composition [15–17]. Various preparative approaches have been proposed to tailor their morphological and physical properties [17], including colloidal [3,18], template [19,20], and supramolecular [21–25]. Among these, the supramolecular approach allows hierarchical self-assembly [21,26–29] of molecular components through the optimization of various noncovalent interactions and provides the unique ability to control matter at the molecular level [30–32]. Various noncovalent interactions such as electrostatic, π–π stacking, H-bonding, coordination bonding, and solvophilic/solvophobic effects have been widely exploited for the generation of specific self-assembled materials both in solution and on surfaces. Over the years, chemists have mastered the ability to design and synthesize molecular components featuring preprogrammed electronic and self-assembly properties.

Recently, our groups have undertaken a research program aimed at exploring the possibility to make photoactive nanomaterials by self-assembling chromophoric units bearing complementary H-bonding sites, in particular di(acetylamino)pyidyl and uracylic moieties [33,34]. Indeed, it has been demonstrated [26,35,36] that complementary H-bonding due to its specificity and directionality serves as a versatile tool for the organization and shape tuning of materials at the nanoscale level. The choice of H-bonding sites as di(acetylamino)pyidyl-DAD (donor–acceptor–donor) and uracylic-ADA (acceptor–donor–acceptor) moieties is dictated by the fact that they undergo self-assembly through triple H-bonding with association constants from 10^3 to 10^5 M^{-1} in apolar solvents [37]. In this article, we report a systematic study on the solvent-dependent photophysical properties of chromophoric systems bearing complementary H-bonding units. These studies show that the majority of the molecules undergo self-recognition and self-aggregation in apolar solvents (e.g., cyclohexane, CHX) leading to the formation of spherical nanoparticles with modified photophysical properties. A further tuning of the nanomaterial is achieved through controlled self-assembly between different molecules bearing complementary H-bonding units and proper geometry.

The structures of molecules **1–10** used for the present study are depicted in Chart 1. The investigated molecular modules are essentially π-conjugated phenyleneethynylenes presenting either uracylic or di(acetylamino)pyridyl moieties as their terminal functionality. They can be classified into three categories: (i) molecules bearing uracylic recognition sites functionalized with either anthracene or pyrene chromophoric units; (ii) phenyleneethynylene derivatives equipped with di(acetylamino)pyridyl (DAD) H-bonding sites; (iii) phenyleneethynylene derivatives bearing uracylic (ADA) recognition sites. Phenyleneethynylenes are conjugated organic molecules with rigid geometry and interesting electronic and optical properties, and herein we investigate in detail how the photophysical properties of **1–10** vary, depending on their molecular structure and functionality. These studies suggest that they are excellent chromophores in the UV–vis region, making them candidates for the fabrication of photoactive materials. Furthermore, their terminal uracylic and di(acetoamino)pyridyl functionalities undergo self-assembly and self-organization processes via H-bonding recognition. It is thus demonstrated that, under solvent and temperature control and by selecting molecular modules with specific geometries and chemical functionalization, it is possible to engineer several self-organized nanomaterials of distinctly different shapes such as spheres, vesicles, wires, helical fibers, and rods.

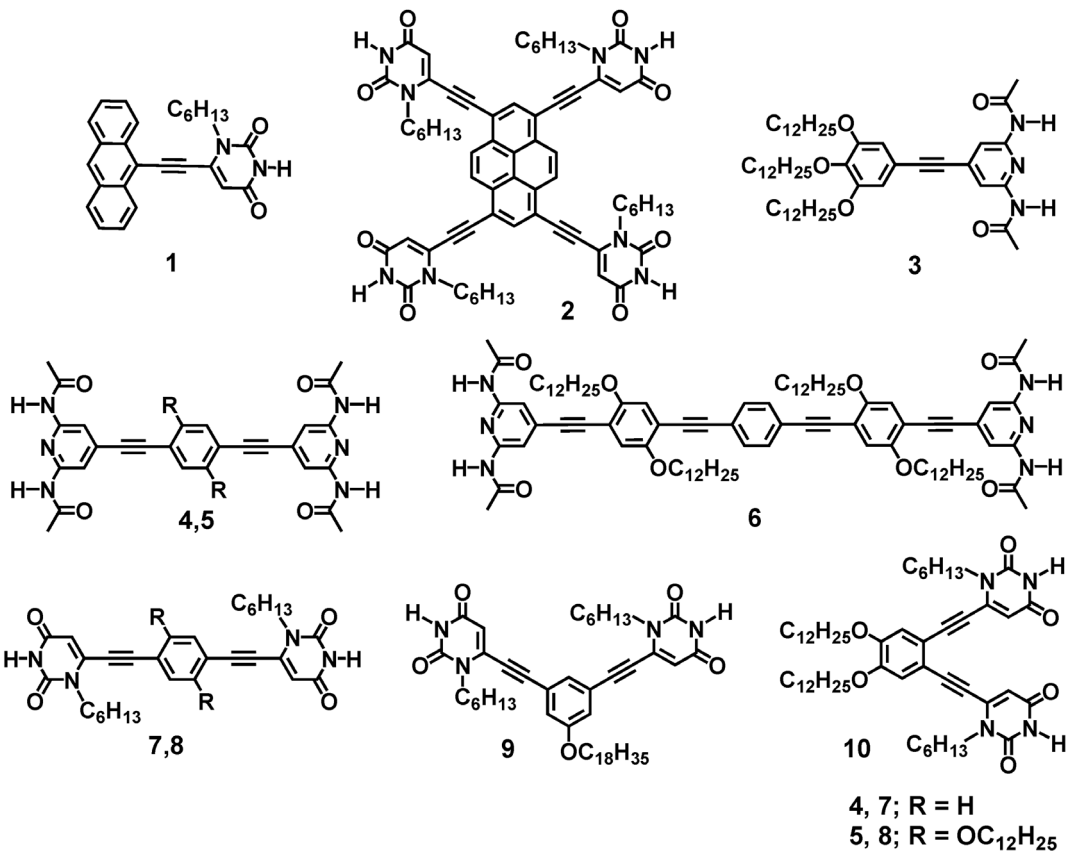

Chart 1 Molecular structure of complementary H-bonding molecular modules. **1**, **2**, **7–10** bear uracylic-ADA recognition sites. **3–6** are equipped with complementary di(acetylamino)pyridil-DAD recognition sites.

EXPERIMENTAL

Solutions for spectroscopic studies were prepared by injecting microlitre amounts (10/20 μL) of 1 mM solutions of each compound in THF into 3 mL of various solvents. Electronic absorption and emission measurements were recorded, respectively, on a Lambda 950 UV/VIS/NIR spectrophotometer (Perkin Elmer) and on a Edinburgh FLS920 spectrofluorimeter (continuous 450 W Xe lamp), equipped with a Peltier-cooled Hamamatsu R928 photomultiplier tube (185–850 nm). The temperature of the solutions was varied with HAAKE F3-C digital heated/refrigerated water bath (Haake Mess-Technik GmbH u.Co., Germany) which can be manually connected to a cuvette holder and controlled externally. Emission quantum yields were determined according to the approach described by Demas and Crosby [38] using quinine sulfate ($\Phi_{em} = 0.546$ in air-equilibrated acid water solution, 1 N H_2SO_4) as standard. All solvents, namely, cyclohexane (CHX), toluene (TOL), carbon tetrachloride (CCl_4), tetrahydrofuran (THF), dichloromethane (DCM), trichlorobenzene (TClB), dimethylsulfoxide (DMSO), benzonitrile (BZN), and methanol (MeOH) are spectroscopic-grade Carlo Erba, (99.8 %) and were used as received.

The samples for wide-field fluorescence microscopy (WFM) were prepared by spin coating ~20 μL of solution on to a microscope glass slide and mounted on an inverted OLYMPUS microscope. The samples were then irradiated through 100X objective lines (NA 1.4) using a 400-nm laser. The emission from the sample was collected through the same objective lens and filtered from excitation light using a dichroic mirror (450 nm) and fed to a CCD camera.

The samples for transmission electron microscopy (TEM) studies were prepared by drop casting ~20 μL of self-assembled solutions on to a carbon coated nickel grid (3.00 mm, 200 mesh), air-dried and imaged on a TEM Philips EM 208 microscope (accelerating voltage of 100 kV).

Tapping-mode AFM measurements (TM-AFM) of the samples deposited on mica substrates were made in air at 298 K, using a Nanoscope IIIa (Digital Instruments Metrology Group, USA) instrument, model: MMAFMLN. The tips used in all measurements were phosphorous-doped silicon cantilevers (T = 20–80 μm, L = 115–135 μm, f_o = 200–400 kHz, k = 20–80 N m^{-1}, VEECO, USA) at a resonant frequency of ca. 300 kHz. The collected images were then analyzed with both Nanoscope and WsXm 4.0 software (Nanotec Electronica S. L.) [39].

RESULTS AND DISCUSSION

Photophysical properties

*Molecules **1** and **2***

The absorption and emission spectra of **1** and **2** in various solvents are depicted in Fig. 1. For the anthracene derivative **1**, the lowest-energy absorption band is located at 437 nm (ε = 10 300 M^{-1} cm^{-1}) in CH_2Cl_2 and the overall spectral shape is little affected by solvent polarity even though the spectral onset is progressively red-shifted with the medium polarity (Fig. 1a). This solvent-dependent trend is amplified in the emission spectra where a pronounced vibronic structure is observed in CHX (Fig. 1a, λ_{max} = 441 nm). Upon increasing the solvent polarity, this shape is gradually lost until a red-shifted, broad, and structureless band is found in MeOH (λ_{max} = 490 nm). This is rather different with respect to what is observed for pristine anthracene, which exhibits structured emission spectra both in apolar and in polar solvents such as acetonitrile and MeOH [40]. The observed trend for **1** suggests that the lowest electronic transition is changed from purely π–π* to partial charge transfer by increasing the polarity of the environment.

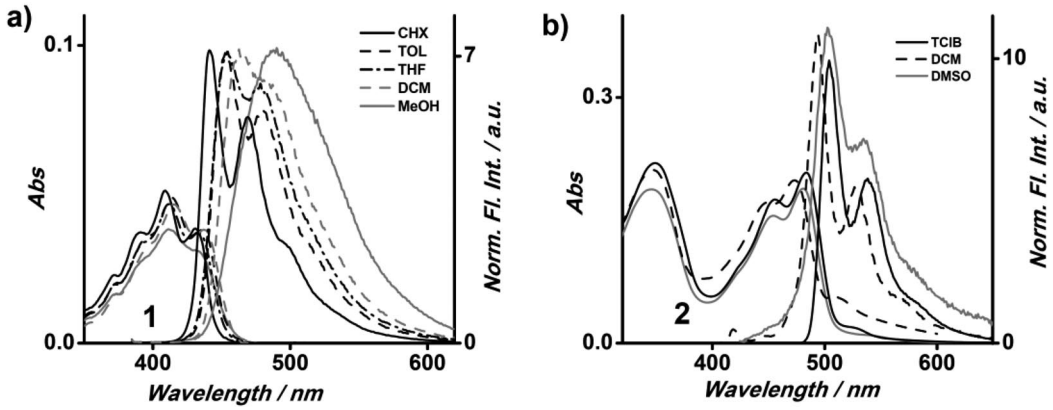

Fig. 1 Absorption and normalized fluorescence spectra of 3.3 μM **1** (a) and 7.2 μM **2** (b) in solvents of different polarity. Emission spectra were collected after exciting at 375 and 308 nm for **1** and **2**, respectively.

The poor solubility of **2** in several solvents made it difficult to investigate in detail the solvent-dependent properties. Absorption and emission spectra of **2** in selected media (TClB, DCM, DMSO) is gathered in Fig. 1b and shows a negligible effect of solvent polarity, as expected based on the π–π* nature of electronic transitions of pyrene [41,42] and the high symmetry of the molecule that cannot promote intramolecular charge-transfer transitions. The lowest-energy absorption band envelop of **2** peaks at 474 nm (ε = 27,600 M^{-1} cm^{-1}) and is a good mirror image of the fluorescence spectrum

(λ_{max} = 494 nm). The fluorescence quantum yield (Φ_{fl}) is 0.44 and the singlet excited-state lifetime is 1.5 ns, i.e., substantially shorter than that of unsubstituted pyrene as monomer (τ_{fl} = 20 ns in air-equilibrated CHX solution) [42].

*Molecule **3***

Molecule **3** is the smallest phenyleneethynylene derivative and possesses only one H-bonding (DAD) unit. The absorption and fluorescence spectra of this molecule in different solvents are depicted in Fig. 2 and show a trend similar to that of monotopic system **1**. A progressive red-shift of the absorption onset and of the emission spectra suggest an increasingly polar character of the lowest electronic excited state, which can be related to the presence of a charge-transfer process from the trialkoxy-substituted phenyl ring to the di(acetylamino)pyridyl moiety.

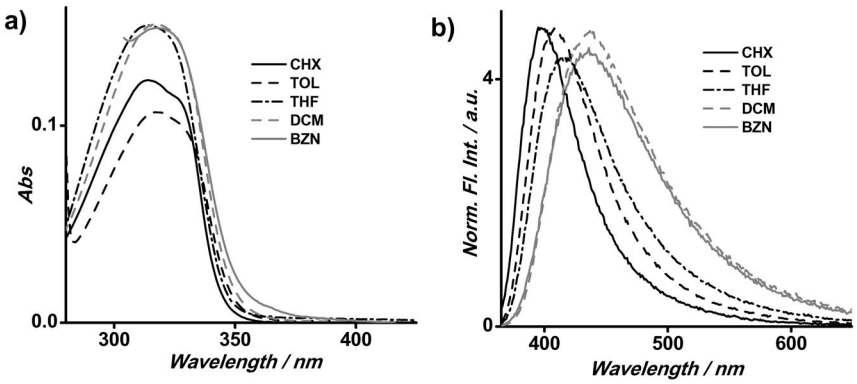

Fig. 2 Absorption (a) and normalized emission (b) spectra of 5.5 μM **3** in solvents of varying polarity. Emission spectra were collected after exciting at 331 nm.

Table 1 Photophysical properties of phenyleneethynylene derivatives bearing di(acetylamino)pyridyl functionalities (**3–6**) in various solvents.

	3		**4**		**5**		**6**	
Solvents	Φ_{fl}	τ_{fl} (ns)	Φ_{fl}	τ_{fl} (ns)	Φ_{fl}	τ_{fl} (ns)	Φ_{fl}	τ_{fl} (ns)
CHX	–	–	0.003	–	0.03	–	0.09	–
TOL	0.24	1.5	0.18	1.1	0.72	2.0	0.67	0.9
THF	0.14	1.7	0.16	2.8	0.95	2.1	0.75	0.9
DCM	0.09	1.4	0.18	1.4	0.99	2.2	0.73	1.1
BZN	0.08	1.6	0.17	3.9	0.76	2.1	0.7	1.0

*Molecules **4–6***

These molecules are linear phenyleneethynylenes equipped with di(acetylamino)pyiridyl-DAD terminal units. They differ each other in the length of the phenyleneethynylene backbone and in the presence or absence of alkoxy chains on phenyl rings. The absorption and emission spectra of **4–6** in various solvents are shown in Fig. 3. In general, they exhibit negligible shifts in their maxima upon varying the solvent polarity (except for CHX, vide infra). Structurally, these molecules have a symmetric geometry with identical di(acetylamino)pyridyl groups at both ends, lacking the possibility of intramolecular charge transfer. Hence it is concluded that the lowest electronic transitions originate from apolar π–π* transitions. It has to be noted that the poor solubility of **4** in a wide variety of solvents prevented an extensive characterization as a function of solvent polarity. In CH_2Cl_2, **4** exhibits a broad and partially

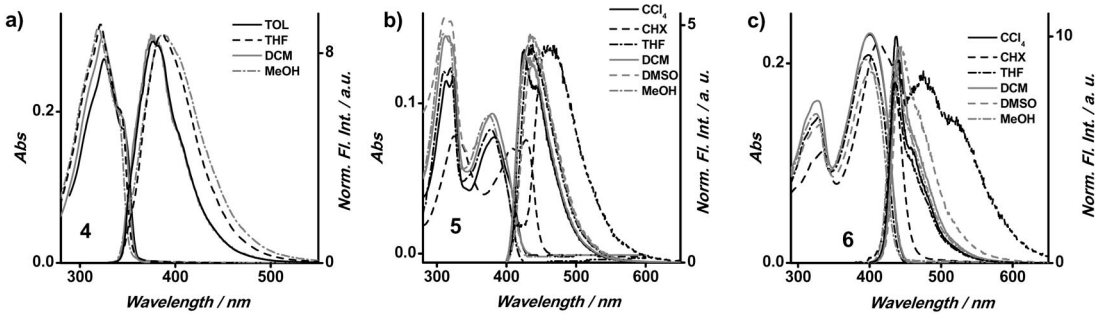

Fig. 3 Absorption and normalized fluorescence spectra of 6.7 μM **4** (a), 3.3 μM **5** (b), and 3.3 μM **6** (c) in various solvents. Emission spectra were collected after exciting at 295, 370, and 360 nm for **4**, **5**, and **6** respectively.

resolved absorption with maximum around 324 nm ($\varepsilon = 43\,900$ M^{-1} cm^{-1}) and a fluorescence maximum around 375 nm, with a relatively high quantum yield of 0.43 and an excited-state lifetime of 1.3 ns. In contrast, the absorption spectra of **5** and **6** show more pronounced features with two well-separated bands. Molecule **5** has the same phenyleneethynylene core unit as **4** yet bearing two alkoxy chains; it exhibits a higher energy and partially resolved band at 315 nm and a low-energy red-shifted absorption around 380 nm ($\varepsilon = 28\,200$ M^{-1} cm^{-1}). Notably, this molecule exhibits also an intense emission with maximum at 425 nm and has a virtually unitary fluorescence quantum yield ($\Phi_{fl} = 0.99$, $\tau_f = 2.1$ ns). This difference in the electronic properties between the two molecules is attributed to the resonance interaction of the oxygen lone pairs with the aromatic π-orbitals [43]. A further red-shift of the absorption and emission features is observed for **6**, which is in agreement with the increase of the length of the phenyleneethynylene backbone.

Surprisingly, **5** and **6** exhibit markedly red-shifted absorption and emission features solely in CHX, which can be attributed to π–π stacking arising from a self-aggregation process (vide infra).

*Molecules **7–10***

This group comprises molecular modules bearing uracylic-ADA moieties as H-bonding recognition sites. They can be further classified into two subgroups; molecules possessing (i) linear (**7** and **8**) and (ii) angular (**9** and **10**) geometry. Similarly to their di(acetoamino)pyridyl counterparts **4** and **5**, molecule **7** exhibits a broad absorption with maximum around 345 nm (Fig. 4a) while molecule **8** has two bands with maxima around 325 and 400 nm (Fig. 4b). This difference in electronic features between **7** and **8** is attributable to the presence of two alkoxy chains on the backbone of **8** (see above) [43]. **7** exhibits a more structured emission profile with maximum around 395 nm ($\Phi_f = 0.11$ and $\tau_f = 0.4$ ns), which is rather independent of the solvent polarity. **8** exhibits a red-shifted and rather featureless emission with quantum yields as high as 0.8 ($\lambda_{max} = 450$ nm, $\tau_f = 1.8$ ns in THF) and shows a weak solvatochromism of 25 nm upon changing the solvent from TOL to BNZ, indicating a polar nature of the excited state.

Compared to their linear counterparts, the two molecular modules showing a bent geometry (**9** and **10**) have blue-shifted absorption and emission features (Figs. 4c,d), indicating a decrease of electronic conjugation. For example, **9**, in which the uracyl units are connected at *meta*-positions (120°), displays an absorption maximum at 320 nm with a small shoulder at 350 nm (Fig. 4c). It has to be noted that, over the whole series, **9** has the lowest emission quantum yield ($\Phi_f = 0.02$, $\tau_f = 2.3$ ns). The spectroscopic studies in various solvents show that **9** is negligibly affected by the medium polarity, on passing from TOL to BZN. Similar to the previous cases, this molecule displays red-shifted absorption *only* in CHX suggesting the presence of π–π stacking interactions arising from aggregation. Very interestingly, **9** exhibits highly enhanced emission quantum yields in CHX ($\Phi_{em} = 0.4$) attributable to aggre-

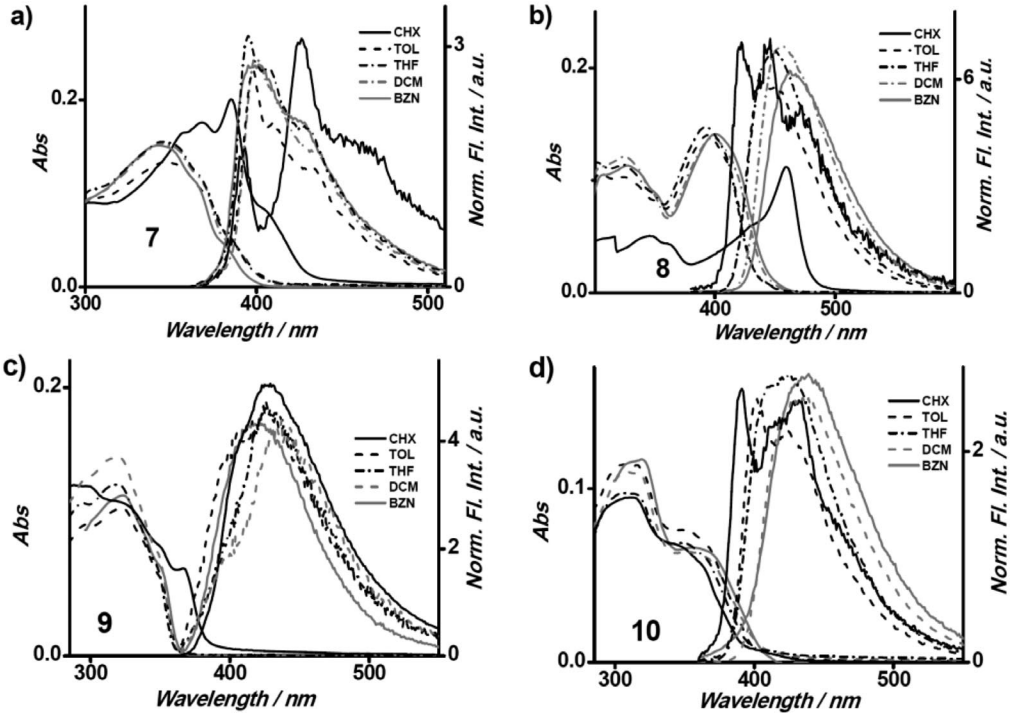

Fig. 4 Absorption and fluorescence of 5.6 μM **7** (a), 5.7 μM **8** (b), 4.5 μM **9** (c), and 4.3 μM **10** (d) in various solvents. Emission spectra were collected after exciting at 331 nm.

gation-induced emission enhancement, as observed elsewhere for biphenyls [44,45], tetraphenylethenes [46], stilbenes [47], and tetraphenyl siloles [48,49].

Molecule **10**, with the H-bonding sites in *ortho*-positions (60º), has an absorption maximum around 315 nm (Fig. 4d) with a shoulder at 353 nm, which is also negligibly affected by solvent polarity. On the contrary, **10** shows a structured emission band with maximum at 400 nm in TOL ($\Phi_f = 0.18$), which red-shifts by 40 nm and becomes featureless in BZN ($\Phi_f = 0.23$). **10** exhibits quenched emission in CHX ($\Phi_f = 0.07$) indicating the formation of aggregates as in the case of other molecules (see above).

Formation of supramolecular nanoaggregates

The UV–vis absorption and emission spectra of molecules **1–9** recorded in different solvents (vide supra) show that most of them exhibit red-shifted absorption and emission profiles in apolar CHX. This is attributed to the π–π stacking interactions arising from the self-aggregation leading to the formation of nano/micro particles. The self-aggregation behavior of these molecules in CHX is further confirmed through variable temperature experiments and the obtained nano/micro materials have been characterized using AFM, TEM, and WFM microscopic techniques. The tuning of the shape of these nanomaterials through complementary H-bonding interactions has been investigated, and the obtained results are discussed in detail in the following sections.

Spherical nanoparticles

Figures 5a–c gather the absorption and emission spectral changes of molecular module **5** in CHX as a function of temperature. Upon increasing the temperature from 298 to 350 K, both the absorption and emission spectra undergo a gradual blue-shift. For example, at room temperature, the linear linker **5** displays the lowest-energy absorption feature at 415 nm which, upon increasing the temperature to 353 K,

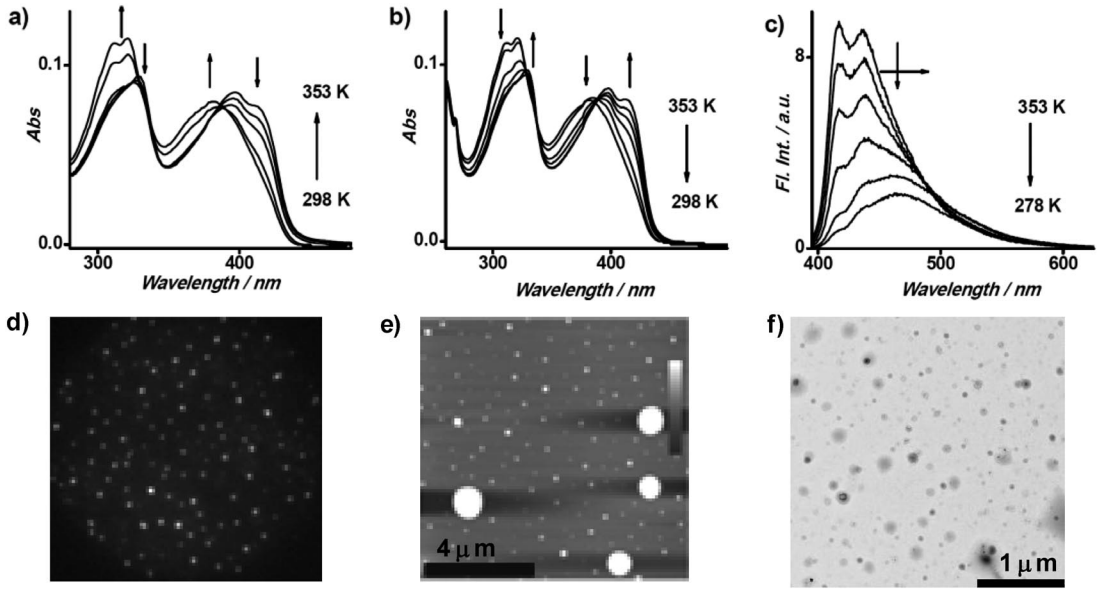

Fig. 5 Absorption (a,b) and emission (c) of 3.3 μM **5** in CHX upon heating (a) and cooling (b,c) cycles. Emission spectral changes were collected upon excitation at 390 nm. WFM (d), AFM (e), and TEM (f) microscopic images of the nanomaterial obtained via self-aggregation of module **5**.

undergoes gradual hypsochromic shift to 380 nm (Fig. 5a). These spectral changes are completely reversible upon cooling the system (Fig. 5b), with a red-shift of their absorption maximum. In line with these changes during the heating cycle, the emission spectrum gains in intensity and shows a blue-shift of its peak; upon cooling, the fluorescence signal is gradually quenched with a continuous red-shift from 415 to 470 nm (Fig. 5c). WFM images (Fig. 5d) recorded from different areas of the sample indicate that, in CHX, molecule **5** self-organizes and forms bright luminescent particles (upon irradiation with 400-nm laser) with different size. Similar nano/micro-sized particles are observed both in AFM (Fig. 5e) and TEM (Fig. 5f) analysis. The cross-sectional analysis of these images indicates that the size of the particles typically varies from ~20 nm to above 1 μm.

A quite similar spectroscopic behavior has been observed for the other linear linkers **6**, **7**, and **8** in CHX. All of them exhibit red-shifted absorption features at low temperature, which undergoes blue-shift upon heating the solution from 298 to 353 K (Figs. 6a–c). These absorption spectral changes are completely reversible upon cooling the sample. The typical AFM images presented in Figs. 6d–f indicate that all of them undergo self-organization in CHX leading to the formation of nano/micro particles. It is interesting to note that among the series **5–8**, molecular module **6** form nanoparticles having much more uniform size distribution with typical sizes ranging from 80–200 nm. Structurally, these molecules possess a central apolar phenyleneethynylene part and two polar di(acetylamino)pyridyl terminal functionalities. In an apolar solvent like CHX, due to the solvophobic effects, molecules **5–8** undergo self-aggregation leading to the formation of spherical particles. Due to the presence of a larger percentage of solvophilic structure, the nanoparticles formed from extended linear module **6** exhibit narrow size distribution. The observed spectral red-shifts at low temperatures in CHX are attributed to the π–π stacking interactions, which is usually the case with J-type aggregates [15,17,34,50].

Further modification of their shape can be achieved through tuning of these solvophilic/solvophobic effects via complementary H-bonding interactions between molecules having different functionality and geometry.

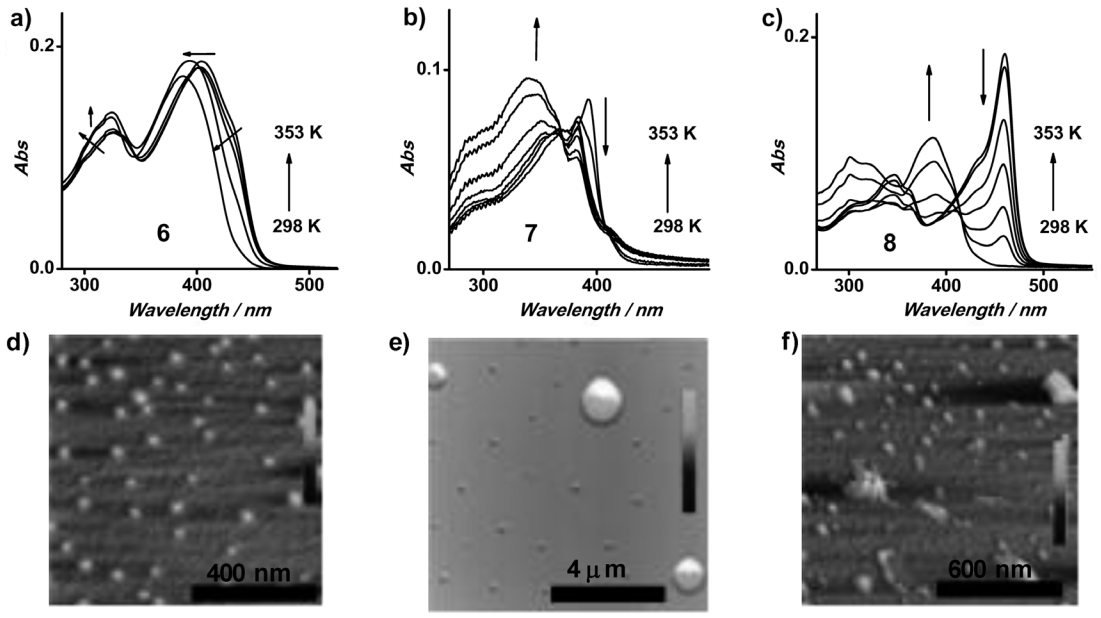

Fig. 6 Absorption spectral changes of 2.7 μM **6** (a), 3.5 μM **7** (b), and 4.2 μM **8** (c) in CHX during heating (a,b) cycles. AFM images of self-organized nano/micro particles of **6** (d), **7** (e), and **8** (f).

Vesicular nanostructures

Structurally, molecule **1** possesses one anthracene unit and one uracilic-ADA moiety that is able to establish complementary H-bonding interactions with the complementary ditopic linear-DAD modules **5** or **6**. The 2:1 molar self-assembly of **1** with either **5** or **6** in CHX results in a dramatic change of the nature of the peripheral functionalities from solvophobic to solvophilic and hence one can expect a change in the shape of resulting nanomaterial [34]. A solution containing 6.6 μM of **1** and 3.3 μM of **5** in CHX displayed new red-shifted absorption and emission features at 465 and 565 nm, respectively (Figs. 7a,b), which are absent in the case of individual molecules (Figs. 1a and 3b). These new red-shifted absorption and emission bands are attributed to the π–π stacking interactions of the anthracenyl derivative initiated by the H-bonding interaction between the uracil-ADA and the 2,6-di(acetylamino)pyridyl-DAD moieties. This aspect was further investigated by recording absorption and emission spectral changes as a function of temperature (Figs. 7a,b). Upon increasing the temperature to 353 K, the low-energy absorption band at 465 nm gradually disappears with a concomitant blue-shift of the whole absorption spectra (Fig. 7b). These spectral changes are fully reversible upon cooling the system, thus confirming that the π–π stacking arises from the self-assembly and aggregation processes.

The WFM image (Fig. 7c) of the resulting nanomaterials showed the presence of bright hollow luminescent circular-shaped aggregates. Similar structures are also observed in TEM images (Fig. 7d) and are attributed to the vesicular structures. The rationale for the formation of nanovesicles can be explained through the establishment of complementary H-bonding interactions that invert the character of the end functionality of the supramolecular adduct from solvophobic (di(acetylamino)pyridyl) to solvophilic (anthracenyl) prompting the formation of vesicular hollowed structures.

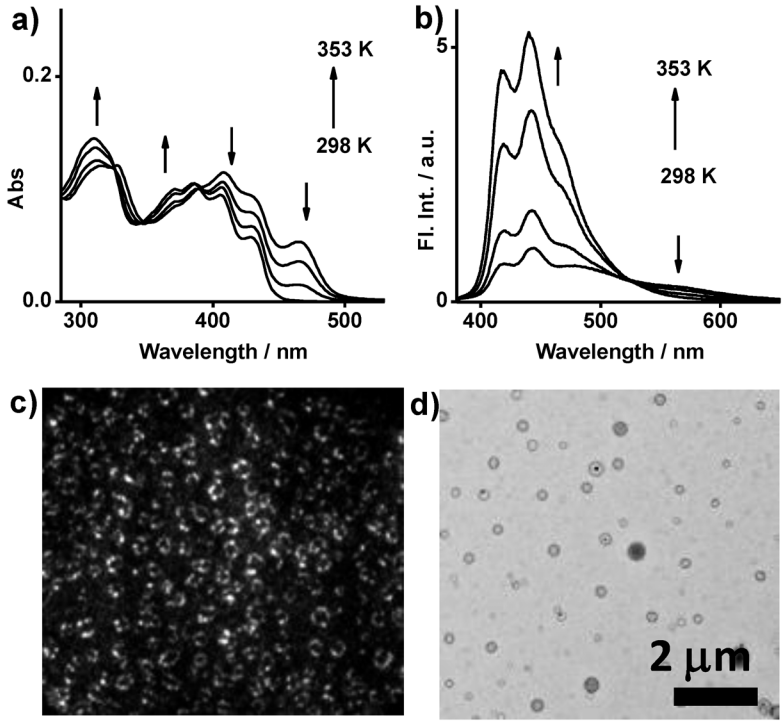

Fig. 7 Absorption (a) and emission (b; λ_{exc} = 347 nm) spectra of a solution containing 6.6 μM of **1** and 3.3 μM **5** in CHX as function of temperature. WFM (c) and TEM (f) images of self-assembled nanostructures of [**5**•(**1**)$_2$].

Nanoparticles to nanowires: Effect of molecular geometry

To probe further the effect of linear complementary H-bonding interactions, we investigated the self-assembly and aggregation behavior of molecule **5** (DAD) with ditopic ADA-molecules having different geometry **7–10**. Molecules **7–10** are similar in composition and in the number of H-bonding sites, but differ in their relative position. Molecules **7** and **8** are linear modules, and the uracylic units are placed at the *para* (180º) position of the central benzene ring. On the other hand, molecules **9** and **10** present the H-bonding sites at *meta* (120º) and *ortho* (60º) positions respectively. In principle, the complementary H-bonding interactions established between the ditopic modules can result in extended supramolecular polymers. Yet, the geometry of the involved molecules **7–10** may have an effect on the shape of the resulting nanomaterial. To study such effects, a 1:1 molar ratio solution containing the DAD-module **5** and complementary ADA-modules **7–10** was prepared in either TOL or CHX (4 % THF), and the UV–vis absorption and emission spectral changes of the resulting nanomaterial were investigated as a function of temperature (Fig. 8). Spectroscopically, all of these molecular assemblies behave in a quite similar fashion; at low temperatures they exhibit a red-shifted absorption band around 420 nm, which gradually disappears with the increase in temperature and the whole absorption spectra blue-shifts. In line with these observations, the molecular assemblies exhibit a quenched emission, which gradually regains its intensity by increasing the temperature. The observed red-shifted absorption and quenched emission at low temperatures are attributed to π–π stacking and the formation of nano-aggregates, which are disrupted at higher temperatures.

The shape of the resulting supramolecular polymeric aggregates was evaluated using AFM (Fig. 8). The complementary H-bonded [**5**•**7**]$_n$ system (Figs. 8b,c) aggregates as supramolecular nanowires with lengths above 400 nm and widths ~30 nm. Interestingly the AFM images recorded for

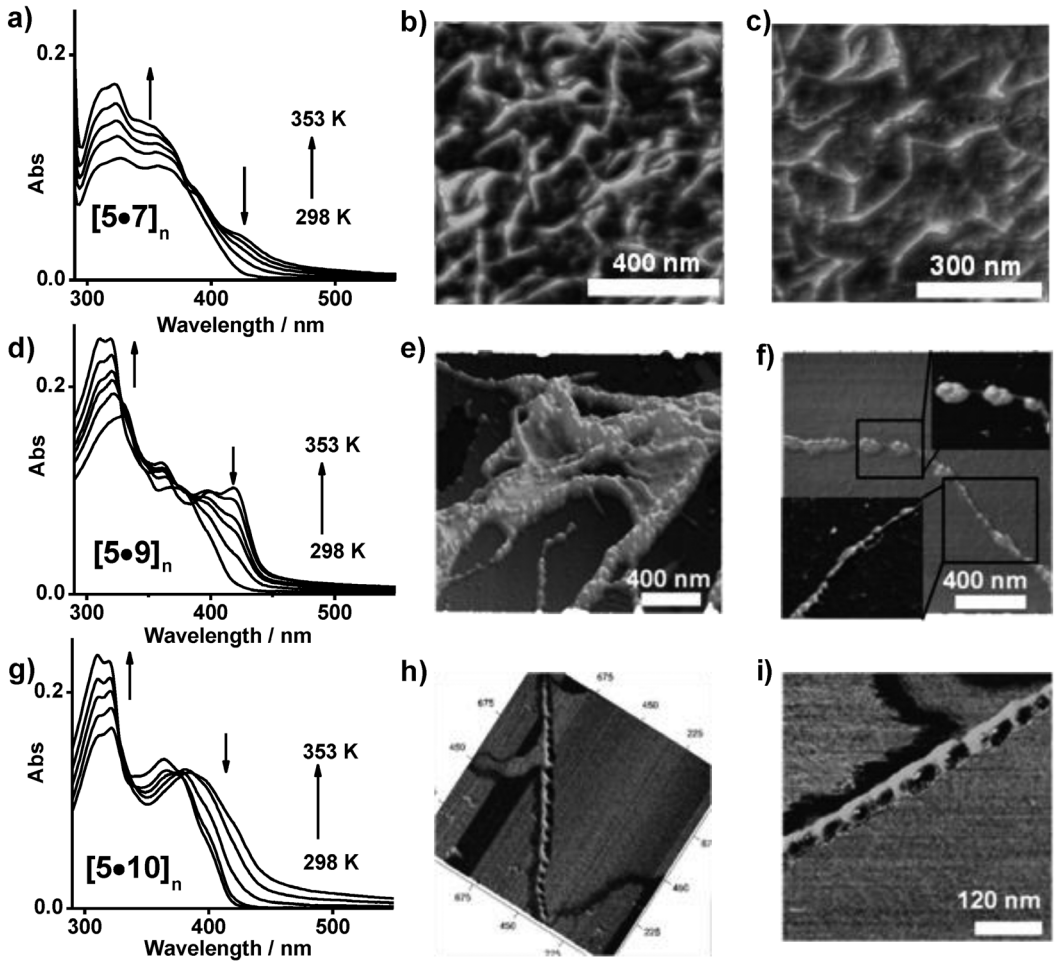

Fig. 8 Absorption (left) spectral changes as a function of temperature and AFM images (right) of (a–c) $[\mathbf{5•7}]_n$ in TOL, (c,d) $[\mathbf{5•9}]_n$ in CHX (4 % THF) and (e,f) $[\mathbf{5•10}]_n$ in CHX (4 % THF) assemblies.

$[\mathbf{5•9}]_n$ (Figs. 8e,f) and $[\mathbf{5•10}]_n$ (Figs. 8h,i) displayed the presence of nanofibers having humps and lumps at regular intervals suggesting a helicoidal organization of the nanostructures. Typically, these helical nanofibers possess lengths of several μm, widths of 30–50 nm, and show periodicity of the height features of 30–40 nm and 60–80 nm for the $[\mathbf{5•9}]_n$ and $[\mathbf{5•10}]_n$ assemblies respectively.

Nanowires to nanorods

To furher elucidate the power of complementary H-bonding interactions on the self-assembly and the shape of the resulting nanomaterials we combined three different molecular components **1**, **5**, and **7**. In the previous section, it is shown that the $[\mathbf{5•7}]_n$ supramolecular polymer forms nanofibers. The addition of a third molecular component such as anthraceynyl derivative **1**, which has only one H-bonding site, can effectively block the extent of the linear H bonding between **5** and **7**. This may further cause a change in the morphology of the resulting nanomaterial. In order to test this aspect, we combined **1**, **5**, and **7** in the 1:10:10 molar ratio in TOL at 373 K, stirred for 3 min, and slowly cooled to room temperature. The absorption and luminescence properties of this assembly turned out to be substantially identical to that of $[\mathbf{5•7}]_n$ supramolecular system. On the contrary, both the AFM and TEM images (Fig. 9) recorded for this mixed system clearly show the presence of a large portion of nanorods along

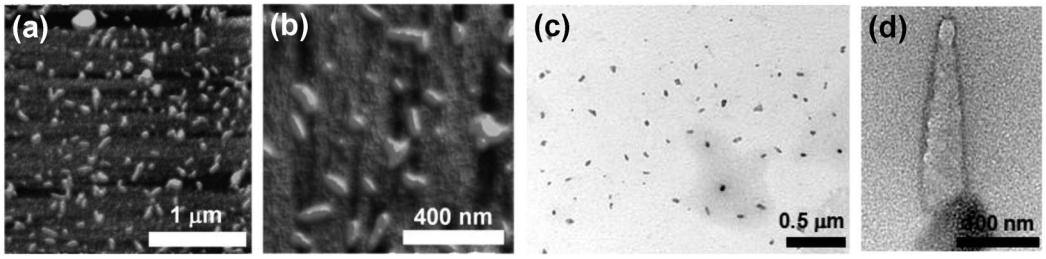

Fig. 9 (a,b) TM-AFM and (c,d) TEM images of the nanorods obtained via self-assembly/self-organization of molecular modules **1**, **5**, and **7** in the ratio 1:10:10.

with some amounts of spherical aggregates. The typical length and width of the rods are 80–200 and 40–60 nm respectively.

CONCLUSIONS

A library of 10 molecular chromophoric scaffolds (**1–10**) equipped with complementary H-bonding functionalities was designed in an attempt to fabricate novel supramolecular nanomaterials. The photophysical studies show that the various molecular modules are generally good luminophores with quantum yields as high as 0.99. Most of them, under suitable solvent/temperature conditions, undergo self-aggregation leading to the formation of spherical nanoparticles with modified photophysical properties. Under appropriate experimental conditions in terms of solvent, temperature, and stoichiometry, binary/ternary combinations of the different molecular modules form a variety of nanostructures such as vesicles, linear and helical fibers and rods, which are generated as a result of H-bonding recognition and self-organization processes. Due to their excellent photophysical properties and the possibility to tune their morphology, the molecular building blocks **1–10** can be potentially utilized to design photoactive functional nanomaterials. We are currently working along this line.

ACKNOWLEDGMENTS

This work was supported by the European Commission through the Marie-Curie Research Training Network "PRAIRIES", (contract MRTN-CT-2006-035810, the Marie-Curie Initial Training Network "FINELUMEN", grant agreement PITN-GA-2008-215399), CNR (commessa PM.P04.010, MACOL), INSTM, the Belgian National Research Foundation (FRS-FNRS, through the contracts n° 2.4.625.08, 2.4.550.09 and 2.4.617.07.F), the "Loterie Nationale", the Région Wallonne through the "SOLWATT" program (contract no. 850551), the 'TINTIN' ARC project from the Belgian French Community (contract no. 09/14-023), and the University of Namur.

REFERENCES

1. A. C. Grimsdale, K. Müllen. *Angew. Chem., Int. Ed.* **44**, 5592 (2005).
2. D. M. Guldi, G. M. A. Rahman, F. Zerbetto, V. Georgakilas, M. Prato. *Acc. Chem. Res.* **38**, 871 (2005).
3. A. R. Hirst, B. Escuder, J. F. Miravet, D. K. Smith. *Angew. Chem., Int. Ed.* **47**, 8002 (2008).
4. A. Ajayaghosh, V. K. Praveen. *Acc. Chem. Res.* **40**, 644 (2007).
5. M. R. Wasielewski. *Acc. Chem. Res.* **42**, 1910 (2009).
6. Z. Wang, Z. Chen, L. Xiao, Q. Gong. *Org. Electron.* **10**, 341 (2009).
7. B. Wang, L. Ke, S.-J. Chua. *J. Cryst. Growth* **288**, 119 (2006).

8. A. L. Briseno, T. W. Holcombe, A. I. Boukai, E. C. Garnett, S. W. Shelton, J. J. M. Frechet, P. Yang. *Nano Lett.* **10**, 334 (2010).
9. S. Günes, H. Neugebauer, N. S. Sariciftci. *Chem. Rev.* **107**, 1324 (2007).
10. R. Bhosale, J. Misek, N. Sakai, S. Matile. *Chem. Soc. Rev.* **39**, 138 (2010).
11. D. H. Kim, B.-L. Lee, H. Moon, H. M. Kang, E. J. Jeong, J. Park, K.-M. Han, S. Lee, B. W. Yoo, B. W. Koo, J. Y. Kim, W. H. Lee, K. Cho, H. A. Becerril, Z. Bao. *J. Am. Chem. Soc.* **131**, 6124 (2009).
12. V. Coropceanu, J. Cornil, D. A. da Silva Filho, Y. Olivier, R. Silbey, J.-L. Brédas. *Chem. Rev.* **107**, 926 (2007).
13. S. R. Forrest, M. E. Thompson. *Chem. Rev.* **107**, 923 (2007).
14. C.-C. Chu, G. Raffy, D. Ray, A. D. Guerzo, B. Kauffmann, G. Wantz, L. Hirsch, D. M. Bassani. *J. Am. Chem. Soc.* **132**, 12717 (2010).
15. H.-B. Fu, J.-N. Yao. *J. Am. Chem. Soc.* **123**, 1434 (2001).
16. D. Xiao, L. Xi, W. Yang, H. Fu, Z. Shuai, Y. Fang, J. Yao. *J. Am. Chem. Soc.* **125**, 6740 (2003).
17. Y. S. Zhao, H. Fu, A. Peng, Y. Ma, D. Xiao, J. Yao. *Adv. Mater.* **20**, 2859 (2008).
18. A. Ajayaghosh, V. K. Praveen, C. Vijayakumar. *Chem. Soc. Rev.* **37**, 109 (2008).
19. X.-L. Fang, S.-L. Deng, J. Wang, X.-F. Wang, C. Chen, Y. Li, S.-Y. Xie, R.-B. Huang, L.-S. Zheng. *Chem. Mater.* **21**, 5763 (2009).
20. C. M. Veziri, M. Palomino, G. N. Karanikolos, A. Corma, N. K. Kanellopoulos, M. Tsapatsis. *Chem. Mater.* **22**, 1492 (2010).
21. J. M. Lehn. *Science* **295**, 2400 (2002).
22. Z. Wang, L. Wang, X. Zhang, J. Shen. *Macromol. Chem. Phys.* **198**, 573 (1997).
23. M. Antonietti, S. Förster. *Adv. Mater.* **15**, 1323 (2003).
24. B.-S. Kim, D.-J. Hong, J. Bae, M. Lee. *J. Am. Chem. Soc.* **127**, 16333 (2005).
25. W.-S. Li, A. Saeki, Y. Yamamoto, T. Fukushima, S. Seki, N. Ishii, K. Kato, M. Takata, T. Aida. *Chem. Asian J.* **5**, 1566 (2010).
26. J. M. Lehn. *Proc. Natl. Acad. Sci. USA* **99**, 4763 (2002).
27. F. J. M. Hoeben, P. Jonkheijm, E. W. Meijer, A. P. H. J. Schenning. *Chem. Rev.* **105**, 1491 (2005).
28. P. J. Stang, B. Olenyuk. *Acc. Chem. Res.* **30**, 502 (1997).
29. G. M. Whitesides, M. Boncheva. *Proc. Natl. Acad. Sci. USA* **99**, 4769 (2002).
30. D. Philp, J. Fraser Stoddart. *Angew. Chem., Int. Ed.* **35**, 1154 (1996).
31. G. M. Whitesides, J. P. Mathias, C. T. Seto. *Science* **254**, 1312 (1991).
32. G. Whitesides. *Small* **1**, 172 (2005).
33. A. Llanes-Pallas, C. A. Palma, L. Piot, A. Belbakra, A. Listorti, M. Prato, P. Samorì, N. Armaroli, D. Bonifazi. *J. Am. Chem. Soc.* **131**, 509 (2009).
34. K. Yoosaf, A. Belbakra, N. Armaroli, A. Llanes-Pallas, D. Bonifazi. *Chem. Commun.* 2830 (2009).
35. C. Meier, U. Ziener, K. Landfester, P. Weihrich. *J. Phys. Chem. B* **109**, 21015 (2005).
36. L. J. Prins, D. N. Reinhoudt, P. Timmerman. *Angew. Chem., Int. Ed.* **40**, 2382 (2001).
37. F. Würthner, C. Thalacker, A. Sautter, W. Schärtl, W. Ibach, O. Hollricher. *Chem.—Eur. J.* **6**, 3871 (2000).
38. G. A. Crosby, J. N. Demas. *J. Phys. Chem.* **75**, 991 (1971).
39. I. Horcas, R. Fernandez, J. M. Gomez-Rodriguez, J. Colchero, J. Gomez-Herrero, A. M. Baro. *Rev. Sci. Instrum.* **78**, 013705 (2007).
40. T. F. Kahan, D. J. Donaldson. *J. Phys. Chem. A* **111**, 1277 (2007).
41. K. Kalyanasundaram, J. K. Thomas. *J. Am. Chem. Soc.* **99**, 2039 (1997).
42. D. S. Karpovich, G. J. Blanchard. *J. Phys. Chem.* **99**, 3951 (1995).
43. P. V. James, P. K. Sudeep, C. H. Suresh, K. G. Thomas. *J. Phys. Chem. A* **110**, 4329 (2006).
44. B.-K. An, S.-K. Kwon, S.-D. Jung, S. Y. Park. *J. Am. Chem. Soc.* **124**, 14410 (2002).
45. B.-K. An, S. K. Kwon, S. Y. Park. *Angew. Chem., Int. Ed.* **46**, 1978 (2007).

46. Z. Zhao, S. Chen, X. Shen, F. Mahtab, Y. Yu, P. Lu, J. W. Y. Lam, H. S. Kwok, B. Z. Tang. *Chem. Commun.* **46**, 686 (2010).
47. C. K. Lim, S. Kim, I. C. Kwon, C. H. Ahn, S. Y. Park. *Chem. Mater.* **21**, 5819 (2009).
48. J. Liu, J. W. Y. Lam, B. Z. Tang. *J. Inorg. Organomet. Polym. Mater.* **19**, 249 (2009).
49. Y. Hong, J. W. Y. Lam, B. Z. Tang. *Chem. Commun.* 4332 (2009).
50. F. C. Spano. *Acc. Chem. Res.* **43**, 429 (2010).

